Electron–ion coupling effects on simulations of radiation damage in pyrochlore waste forms

2010 J. Phys.: Condens. Matter 22 225405

(http://iopscience.iop.org/0953-8984/22/22/225405)

IOP Publishing Journal of Physics: Condensed Matter

J. Phys.: Condens. Matter **22** (2010) 225405 (8pp) doi:10.1088/0953-8984/22/22/225405

Electron–ion coupling effects on simulations of radiation damage in pyrochlore waste forms

Ahmed E Ismail[1,3], Jeffery A Greathouse[2], Paul S Crozier[2] and Stephen M Foiles[2]

[1] Sandia National Laboratories, Carlsbad, NM, USA
[2] Sandia National Laboratories, Albuquerque, NM, USA

E-mail: jagreat@sandia.gov

Received 21 January 2010, in final form 23 April 2010
Published 20 May 2010
Online at stacks.iop.org/JPhysCM/22/225405

Abstract

We have performed molecular dynamics simulations of cascade damage in the gadolinium pyrochlore $Gd_2Zr_2O_7$, comparing results obtained from traditional simulation methodologies that ignore the effect of electron–ion interactions with a 'two-temperature model' in which the electronic subsystem is modeled using a diffusion equation to determine the electronic temperature. We find that the electron–ion interaction friction coefficient γ_p is a significant parameter in determining the behavior of the system following the formation of the primary knock-on atom (PKA; here, a U^{3+} ion). The mean final PKA displacement and the number of defect atoms formed is shown to decrease uniformly with increasing γ_p; however, other properties, such as the final equilibrium temperature and the oxygen–oxygen radial distribution function, show a more complicated dependence on γ_p.

(Some figures in this article are in colour only in the electronic version)

1. Introduction

A closed nuclear fuel cycle will require new materials that are capable of both immobilizing high-level nuclear waste and withstanding the effects of its radiation. However, current waste form materials developed for the once-through fuel cycle may not be adequate for the refined radioactive waste produced by a closed fuel cycle. The state-of-the-art in experimental methods to quantify irradiation resistance in waste form materials has been recently reviewed [1, 2].

In recent years, a number of groups have performed experiments to evaluate the behavior of pyrochlores, a family of materials with $Fd3m$ crystal structure. Lang *et al* [3] examined how Ti concentration in gadolinium pyrochlores increases the damage cross section and alters the structure of ion tracks created by swift heavy ion irradiation. The results of Yudinsev *et al* [4] and Patel *et al* [5] suggest that the susceptibility of pyrochlores to radiation damage depends on the relative size of the cations in the crystal structure. Zhang *et al* [6] have found evidence that gadolinium pyrochlores may amorphize when bombarded with C_{60} clusters, but undergo a non-amorphizing order–disorder transition when irradiated with U. Although experiments such as these provide much useful quantitative information regarding the amount and nature of damage sustained by a material upon irradiation, they have not been able to elucidate the mechanisms involved in structural disorder following irradiation.

Atomistic calculations of ion displacement energies and disordering energies at both the quantum and classical levels of theory have shown good agreement with experiment. Trends in pyrochlore disordering energies have been previously calculated using density functional theory [7, 8]. The disorder energy for the transition between the pyrochlore and defect fluorite phases in $Gd_2Zr_2O_7$ was found to be 0.6 eV/f.u. [7]. This energy difference arises from the displacement of all atoms in the simulation cell and cannot be directly compared with experimental displacement energies. However, the reported trends are in good agreement with trends in experimental order–disorder transformation temperatures [9].

[3] Present address: Aachener Verfahrenstechnik, Faculty of Mechanical Engineering, RWTH Aachen University, Aachen, Germany.

Classical molecular dynamics (MD) simulations have been used to calculate atomic displacement energies in similar oxide materials. For zircon, the average cation and oxygen displacement energies of 75 eV and 60 eV, respectively, lie within the range of reported experimental values [10].

Atomistic simulations have also been used to study the damage caused by low-energy irradiation events in ceramic oxide materials [11]. Molecular statics calculations were used to compare trends in antisite defect formation energies in a range of pyrochlores [12], while MD simulations have been used to study accommodation of Pu and U in pyrochlore oxides [13], and to study local disorder energy processes in fluorites [14]. More recently, MD simulations have included a low-energy primary knock-on atom (PKA) to quantify the time evolution of structural disorder following a PKA event [15–17]. Such simulations are based on simple pair potentials to govern the interatomic energies, and various post-simulation analyses are used to compare the material structure before and after the damage cascade.

Although these MD simulations have increased our understanding of material resistance to irradiation, they have omitted essential physics by neglecting the effects of energy losses to inelastic scattering by electrons. In this work, we include such electronic effects through use of a two-temperature model (TTM) molecular dynamics approach, wherein the effects of the electrons are explicitly taken into account. The TTM was first introduced by Caro and Victoria [18], and further developed by Duffy and Rutherford [19, 20]. Duffy *et al* have applied this method to study radiation damage caused by low-energy cascades in Fe and swift heavy ion irradiation in W [21]. More recently, Phillips and Crozier have extended the algorithm to provide better energy conservation than was previously available [22]. The electronic subsystem is represented by solving the heat diffusion equation on a regular finite element mesh, and is coupled to the atomic subsystem through an inhomogeneous finite Langevin thermostat.

We have performed MD simulations on $Gd_2Zr_2O_7$, a natural pyrochlore that is stable over geologic times [2, 23] and therefore has applications as potential waste form materials in a next-generation nuclear fuel cycle. Our initial simulation methodology was designed to reproduce the results of recent PKA simulations of $Gd_2Zr_2O_7$ [24], in which electronic effects were not included. The simulations were then repeated after including electronic heating and scattering effects with a TTM. Other researchers have used a TTM to include the effects of electrons when performing PKA simulations, but to our knowledge no one has done so for nonmetallic materials such as the pyrochlore system studied here. A quartz system has been studied [25], but not in the context of a PKA simulation. The present work shows that inclusion of a TTM in radiation damage simulations has a strong influence on the material defects produced.

We briefly review the model system and methodology in section 2. In section 3, we review the results for the temperature profile of the pyrochlore as a function of various parameters, including the electron–ion coupling strength, as well as the structure of the crystal, including radial distribution functions and defect atom analysis. We briefly summarize our findings in section 4.

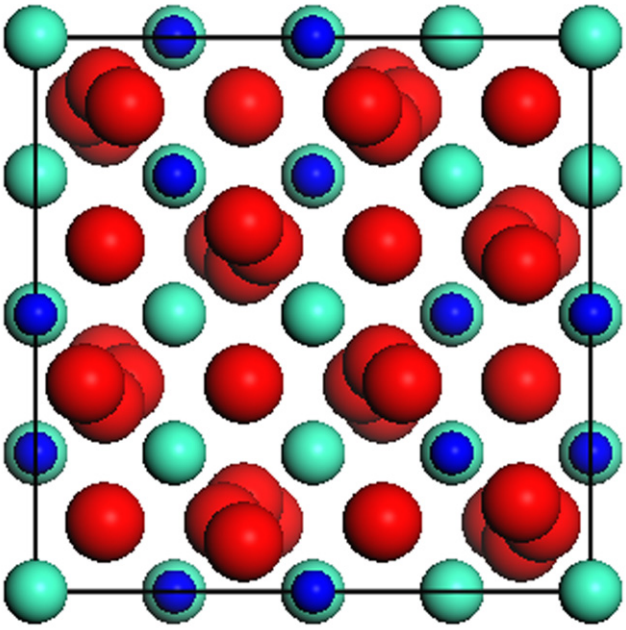

Figure 1. The unit cell of $Gd_2Zr_2O_7$ based on the crystal structure [26] with space group $Fd3m$ (O: large, red atoms; Gd: medium, light blue atoms; Zr: small, dark blue atoms). The edge length is 10.52 Å.

2. Modeling methods

2.1. Pyrochlore model

The model system consists of a gadolinium pyrochlore with the formula $Gd_2Zr_2O_7$. Although based on the fluorite structure, the inclusion of trivalent cations in pyrochlores causes the loss of one oxygen ion per formula unit. The resulting disorder among the oxygen atoms is apparent in the crystal structure shown in figure 1.

Simulations were performed with the LAMMPS molecular dynamics (MD) code [27]. The supercell contained 3375 unit cells (297 000 atoms) of $Gd_2Zr_2O_7$ in a 15 × 15 × 15 grid with an initial supercell length of 157.84 Å. Potential parameters were taken from the literature [15] and consisted of electrostatic interactions with Buckingham (exp-6) parameters for short-range interactions. No bond, angle, torsional, or improper terms were used, and atoms were assigned full ionic charges: O = $-2e$, Gd = $+3e$, and Zr = $+4e$, where e refers to the elementary charge. A short-range cutoff of 10.0 Å was used, and long-range electrostatic interactions were computed with an efficient particle–particle particle–mesh solver [28, 29] with accuracy of one part in 10^5. The equilibrium lattice parameter was first determined with constant pressure simulation using a Nosé–Hoover barostat set to 0 atm with a 500 fs damping constant and a thermostat temperature of 300 K with a 100 fs damping constant. This initial simulation consisted of 5000 steps with a timestep of 2.0 fs. The average unit cell lattice parameter of 10.79 Å is

Table 1. Electron–ion interaction parameters used in the two-temperature model MD simulations.

Property	Value	Justification
Electron specific heat, C_e	0.001 44 kcal mol^{-1} electron^{-1} K^{-1}	Taken from [25] assuming material acts as a semiconductor
Electron density, ρ_e	0.781 Å^{-3}	Taken from [25] assuming material acts as a semiconductor
Electron thermal conductivity, κ_e	0	Appropriate for semiconductor approximation
Electron–ion interaction friction coefficient, γ_p	0.277, 1.385, or 2.77 g mol^{-1} fs^{-1}	Range of values corresponding to relaxation times of 0.2–2 ps, assuming an average molar mass of 608.9 g mol^{-1}
Electron stopping friction coefficient, γ_s	0.2191 g mol^{-1} fs^{-1}	Based on the tables in SRIM 2003 [30] for a 10 keV U atom in $Gd_2Zr_2O_7$
Electron stopping critical velocity	0.0590 Å fs^{-1}	Corresponds to the conventional critical kinetic energy of 10 eV [31]
Number of electronic subsystem grid cells	1000	Corresponds to a 10 × 10 × 10 cubic grid

in good agreement with the experimental value of 10.53 Å obtained by Moriga *et al* [26].

2.2. Primary knock-on atom simulations

PKA simulations were performed in the microcanonical ensemble. The initial configuration, including atomic velocities, was taken from the constant pressure simulation, so that the initial atomic temperature was 300 K. The PKA simulation was initiated by replacing a Gd^{3+} ion with a U^{3+} ion. The PKA was assigned an initial velocity corresponding to a kinetic energy of 10.0 keV. A set of 20 replicate runs were performed, each with a different direction for the initial velocity vector of the PKA chosen at random. A variable timestep algorithm was used to ensure that no atom traveled farther than 0.1 Å in a single timestep, with minimum and maximum timestep values set to 0.001 fs and 2.0 fs, respectively. These variable timestep settings are consistent with a previous study [24] that we used to validate our method. To prevent drift of the atomic system as a result of PKA movement, the atomic system was recentered every timestep, and the net linear momentum of the atoms was also zeroed every timestep.

TTM molecular dynamics consists of a simulation using regular force field parameters to represent the atoms, with a continuum model to represent the electrons. The heat equation is solved numerically on a regular grid, and represents the thermal evolution of the electronic subsystem. In the present work, except where noted, we used a 10 × 10 × 10 cubic grid, corresponding to approximately 300 atoms per cell. The atomic subsystem is evolved using molecular dynamics. The two subsystems are coupled through an inhomogeneous finite Langevin thermostat as described in [22], wherein the atoms experience Langevin forces representing their interactions with the electrons and energy is exchanged between the two subsystems such that total system energy is conserved.

Accurate TTM parameters for all ion–electron interactions, as well as more precise determinations of the electrical charges to be assigned to the various atoms in $Gd_2Zr_2O_7$, would require extensive quantum calculations that were not part of this initial study. Instead, we adopted a recent approach for TTM simulations of quartz [25] in which the material was treated as a semiconductor. The TTM parameters and their justification are given in table 1.

3. Results and discussion

3.1. Validation of methodology

We first validated our MD simulation methodology by comparing results for a PKA cascade in $Gd_2Zr_2O_7$ with the literature [24]. Electronic effects were not included in this comparison. Specifically, we calculated average atomic displacements from a set of eight simulations with a 10 keV PKA atom directed along each of the eight body diagonals of a 13 × 13 × 13 supercell. The average number of Gd, Zr, and O atoms displaced by at least 1.0 Å were 15.5, 11.4, and 645.6, respectively, which is in excellent agreement with the corresponding values of 15, 12, and 610 from [24]. The average PKA displacement was found to be 130 Å, which is significantly larger than the value of 95 Å reported by Todorov *et al* [24]. However, we obtained an average PKA displacement of 93 Å using wrapped atomic coordinates (i.e., the PKA coordinates are always in the original simulation cell even if it passes through a periodic boundary), so we suspect that a similar method was used by Todorov *et al* [24] to calculate their PKA displacements. The true average displacement of 130 Å is very close to the supercell lattice parameter 136.8 Å, so all subsequent simulations were performed with a larger 15 × 15 × 15 supercell (157.8 Å). Results for this larger supercell are discussed below.

3.2. Temperature profiles

Temperature profiles as a function of time for the four different choices of model parameter—the original model without electronic subsystem, plus the two-temperature model systems with electron–ion interaction friction coefficient $\gamma_p =$

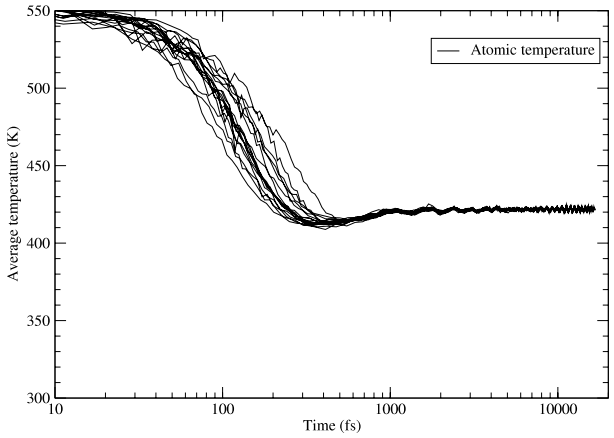

Figure 2. Temperature versus time for $\gamma_p = 0$.

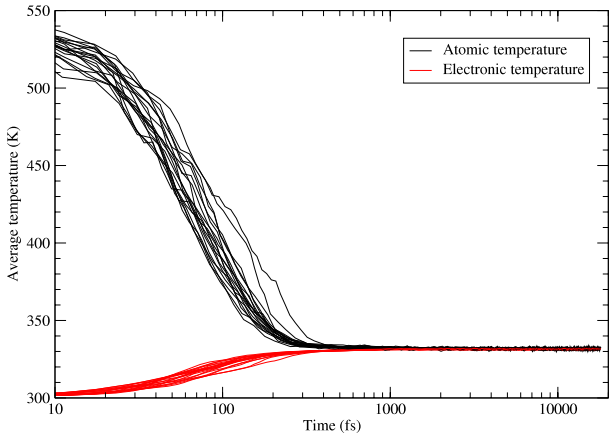

Figure 3. Temperature versus time for $\gamma_p = 0.277$ g mol^{-1} fs^{-1}.

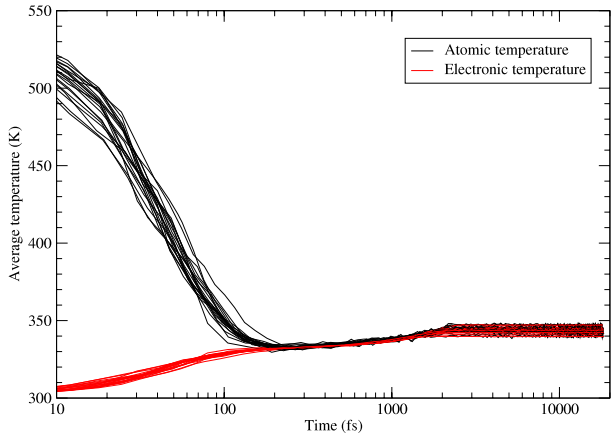

Figure 4. Temperature versus time for $\gamma_p = 1.385$ g mol^{-1} fs^{-1}.

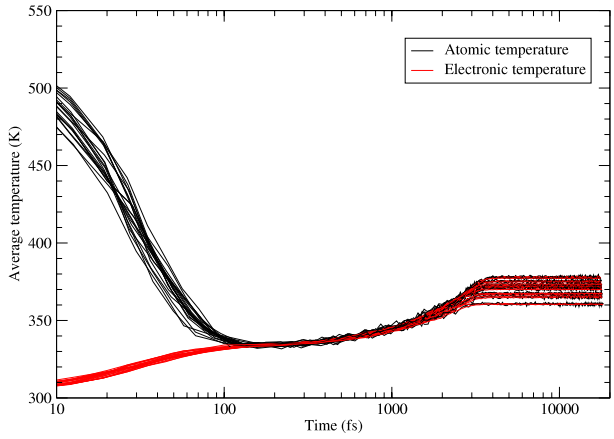

Figure 5. Temperature versus time for $\gamma_p = 2.77$ g mol^{-1} fs^{-1}.

0.277, 1.385, or 2.77 g mol^{-1} fs^{-1}—are shown in figures 2–5. Statistics for the different values of γ_p, averaged over the 20 random vectors for each value, are shown in table 2. Examining the temperature profiles as a function of time, the pyrochlore appears to pass through three different phases during the approximately 15–18 ps of simulation time.

(i) Exponential-rate cooling of the atomic system, accompanied by heating of the electronic subsystem, if present.
(ii) Linear-rate heating of the combined system to the final equilibrium temperature.
(iii) Relatively small fluctuations in the final temperature following equilibration of the lattice.

Both the magnitude of the temperature changes and the length of each phase appear to depend significantly on the electron–ion friction coefficient γ_p. Without the electronic subsystem, the atomic temperature decreases more slowly, and does not cool to as low a temperature: cooling requires as much as 0.5 ps to reach a temperature of 410 K without the electronic subsystem, while the TTM systems reach a minimum temperature of 335 K after approximately 0.2 ps. This minimum appears to be independent of the magnitude of the friction coefficient.

Table 2. Statistics for final temperatures following PKA displacement in $Gd_2Zr_2O_7$ as a function of electron–ion interaction friction coefficient γ_p.

	Mean final temperatures (K)		
γ_p (g mol^{-1} fs^{-1})	Atomic subsystem	Electronic subsystem	Change in total energy (ΔE, Mcal mol^{-1})
0	422.0 ± 0.7	—	0
0.277	331.8 ± 0.3	331.7 ± 0.3	4
1.385	343.8 ± 1.9	344.0 ± 1.9	89
2.77	370.6 ± 4.9	370.6 ± 5.2	268

The duration of the second phase, heating of the combined system as a result of frictional slowing of both the ions and electrons, lengthens as the friction coefficient γ_p between the subsystems increases. The heating period is almost nonexistent for the smallest γ_p considered, as the relatively small value of the coefficient means little of the PKA's kinetic energy will be dissipated by friction and thereby converted to heat. However, the heating phase lasts for nearly 2 ps for $\gamma_p = 1.385$ g mol^{-1} fs^{-1} and almost 3 ps for $\gamma_p = 2.77$ g mol^{-1} fs^{-1}. The duration of the second phase appears to depend primarily on the temperature difference between

Table 3. Statistics for PKA displacement in $Gd_2Zr_2O_7$ as a function of electron–ion interaction friction coefficient γ_p.

γ_p (g mol^{-1} fs^{-1})	Mean final PKA displacement (Å)	Mean number of defect Gd atoms	
		Maximum number	Equilibrium number
0	149 ± 30	694 ± 73	150 ± 48
0.277	109 ± 17	201 ± 36	32 ± 17
1.385	65.5 ± 7.4	153 ± 21	25 ± 13
2.77	44.8 ± 5.4	150 ± 10	25 ± 12

the final equilibrium temperature and the minimum observed temperature after cooling.

The equilibrium temperatures reached by the different systems also depends on the friction coefficient. The non-electron system maintains the highest average final temperature (422 K), while those with electronic subsystems available have temperatures increasing from 332 K for $\gamma_p = 0.277$ to 371 K for $\gamma_p = 2.77$, a consequence of the greater amount of heat released by frictional stopping in both subsystems with increasing values of γ_p. The presence of the electronic subsystem also dampens the oscillations observed in figure 2, so that the temperature remains more stable once equilibrium has been established.

An unexpected trend observed in the two-temperature model simulations is the variability in the final temperatures. As shown in table 3, the standard deviation in the distribution of equilibrium temperatures is a rapidly increasing function of the friction coefficient γ_p, suggesting that while larger friction coefficients lead to smaller PKA displacements, larger variations in the final state of the system also result.

3.3. Energy conservation

To determine how well the two-temperature model conserves energy, the change in energy was computed as a function of time:

$$\Delta E(t) = \Delta U(t) + \Delta K(t) + N_e C_e(\bar{T}_e(t) - \bar{T}_e(0)), \qquad (1)$$

where $\Delta U(t)$ is the change in potential energy, $\Delta K(t)$ is the change in kinetic energy, $N_e = \rho_e V$ is the number of electrons used to absorb heat from the atomic subsystem, and $\bar{T}_e(t)$ is the mean temperature of the electronic subsystem at time t. Because the simulations have been performed in the microcanonical (NVE) ensemble, we expect that the energy drift should be negligible over the course of a simulation. However, because of the numerical approximations introduced as a result of the electronic subsystem, it is possible that small amounts of drift will occur over the course of the simulation.

As shown in table 2, there is minimal drift in the total energy for the system without electronic subsystem, as well as for the two-temperature model with $\gamma_p = 0.277$ g mol^{-1} fs^{-1}. As γ_p increases, however, the drift in total energy becomes significantly more pronounced, reaching approximately 0.1% when $\gamma_p = 2.77$ g mol^{-1} fs^{-1}. This suggests that for the short relaxation times corresponding to the larger values of γ_p, the response of the electronic subsystem to the fast-moving PKA becomes harder to control numerically.

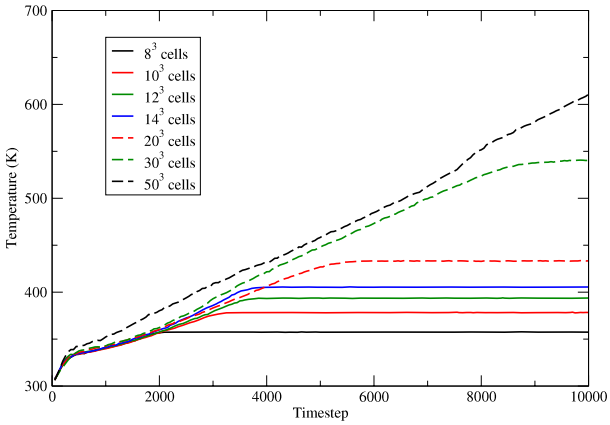

Figure 6. Time evolution of the average electronic temperature as a function of the number of electronic cells for $\gamma_p = 2.77$ g mol^{-1} fs^{-1}.

3.4. Effects of model parameterization

3.4.1. Electronic grid size. The final temperature also appears to depend on the total number of grid cells in the electronic subsystem, as shown in figure 6. As the number of cells in the mesh for electronic subsystem calculations increase, the final temperature of the system also increases. The final temperature in fact does not appear to converge as a function of the mesh density; for instance, the difference in final temperatures for meshes with 10^3 and 20^3 cells is smaller than the difference between meshes with 20^3 and 30^3 cells. Moreover, the increase in the number of cells increases the time required to reach the equilibrium temperature of the simulation.

In the case of fewer grid cells, the electron density in each cell is large enough that atomic energy from the high-velocity atoms can be absorbed with a relatively small change in the electronic temperature. Additionally, the PKA is slowed more quickly when an electronic subsystem is present, so fewer electronic cells experience a substantial change in temperature. As a result, the final temperature (atomic and electronic) is relatively low.

The densest grid considered, 50^3 cells, did not converge to an equilibrium temperature within the 10 000 timesteps simulated. This mesh density corresponds to a system with, on average, less than three atoms per cell. Given the structure of the pyrochlore unit cell, this means that some cells may not contain any atoms at all, which means that no heat should be transferred to those cells. However, the model assumes a uniform electron density, which means that those cells will be considered to be 'occupied', while other cells that contain more atoms will be 'electron-poor' compared to their actual electron density. Moreover, the cell containing the PKA will only be able to transfer its energy to a small number of electrons. Consequently, the cell containing the PKA would be heated to an extremely high temperature, while surrounding cells would remain at temperatures near normal, as the assumption of zero electron thermal conductivity eliminates transfer of energy between adjoining cells in the electronic subsystem.

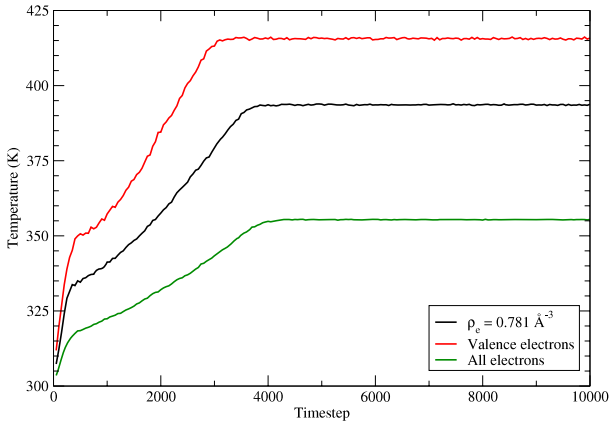

Figure 7. Time evolution of the average electronic temperature as a function of the electron density for $\gamma_p = 2.77$ g mol^{-1} fs^{-1}, using a $12 \times 12 \times 12$ electronic subsystem grid.

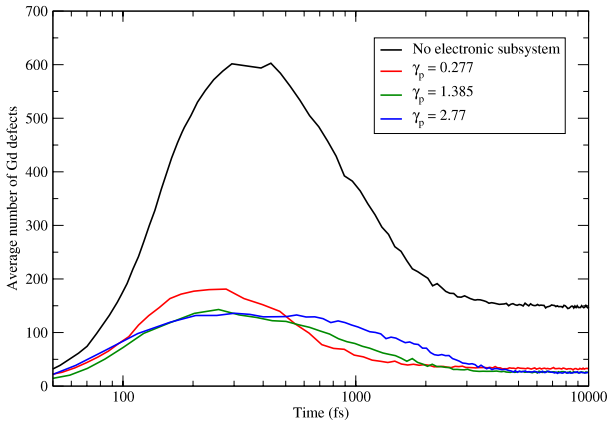

Figure 8. Number of defects as a function of time for a system without electron–ion coupling and for two-temperature model systems with $\gamma_p = 0.277$, 1.385, and 2.77.

3.4.2. Electron density. The density of electrons used in this study represents an intermediate between the two possible extremes that can be used to compute the density of the electronic subsystem. The largest reasonable electron density assumes that all electrons are available, while the lower bound assumes that only the valence electrons found in the outermost orbital shells can interact via the coupling. For the pyrochlore $Gd_2Zr_2O_7$, this corresponds to electron densities between 0.4587 and 1.682 Å^{-3}. The effects of using these different densities are shown in figure 7 for a PKA simulation with $\gamma_p = 2.77$ g mol^{-1} fs^{-1} and a $12 \times 12 \times 12$ grid for the electronic subsystem. As expected, using only the valence electrons to control the heat transfer between the atomic and electronic subsystems leads to a higher final temperature, as less heat can be conducted away from the atomic system.

3.5. Structural analysis

Following the local bond order analysis method of Frenkel and co-workers [32, 33], as well as our previous work with two-temperature models [22, 25], we define a defect atom as one for which the correlation function for the normalized local bond order parameters, $\alpha_j = q_6(i)q_6(j) \geqslant 0.8$ for more than three-quarters of its neighbors in its first coordination shell (approximately 3.6 Å in thickness).

3.5.1. Defect atoms. The average number of defects as a function of time for each value of the friction coefficient γ_p considered is shown in figure 8; the maximum number of defects observed is listed in table 3. The number of defect atoms observed is significantly reduced by the presence of the electronic subsystem: even for $\gamma_p = 0.277$ g mol^{-1} fs^{-1}, there is more than a threefold reduction in the maximum number of defect atoms relative to the system without electronic effects. As the friction coefficient γ_p increases, there is a slight decrease in the equilibrium number of defect atoms; however, the rate of decrease falls off rapidly, and there is essentially no difference in the number of defect atoms between $\gamma_p = 1.385$ and 2.77 g mol^{-1} fs^{-1}. The ratio between the maximum number of defect atoms and the number of defect atoms after equilibration also appears to be qualitatively different for the two different types of systems: while the ratio is approximately 4.5:1 for the system without electronic effects, but approximately 6:1 for nonzero values of γ_p. It further appears that there is a 'saturation' value of γ_p, above which there is little effect on the equilibrium number of defects.

Examining the change in the number of defect atoms as a function of time, we see that the maximum number of defects occurs at around 500 ps for the supercell without electron–ion interactions. Changing the value of the friction coefficient γ_p has an unusual effect on the location of the maximum: for small values of γ_p, the onset of the maximum is earlier than without electronic effects. However, for the largest value of γ_p considered here, the onset actually occurs later. For the TTM simulations, the time at which the equilibrium number of defects is reached is proportional to γ_p.

Comparing these results to the propagation of defect atoms obtained by Rutherford and Duffy using an inhomogeneous thermostat [20], we find rather significant differences in the behavior of the system as a function of γ_p. Rutherford and Duffy find that both the maximum number of defect atoms, as well as the time at which the maximum number of defect atoms occurs, are both strongly decreasing functions of γ_p; our results suggest that the maximum number of defects falls off much more gradually, while the time corresponding to the maximum number of defects actually increases with γ_p. The difference in the results may be the result of the different crystal structures examined: Rutherford and Duffy examined cascade damage in a Fe crystal, which has a significantly simpler crystal structure, with greater void spaces between atoms than the pyrochlore studied here. It is also possible that the imposition of zero thermal conductivity assumed here may also be the source of the difference.

3.5.2. PKA displacements and O–O radial distribution functions. The effect of the friction coefficient γ_p can be most directly observed in the PKA displacement as a function of time for different values of γ_p. Distribution

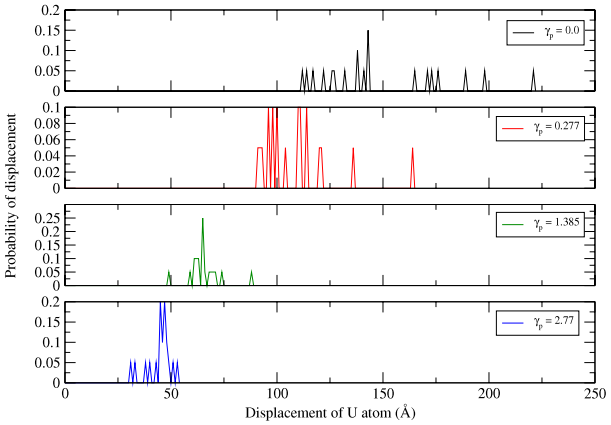

Figure 9. Displacement of PKA atoms after 10 000 timesteps as a function of γ_p.

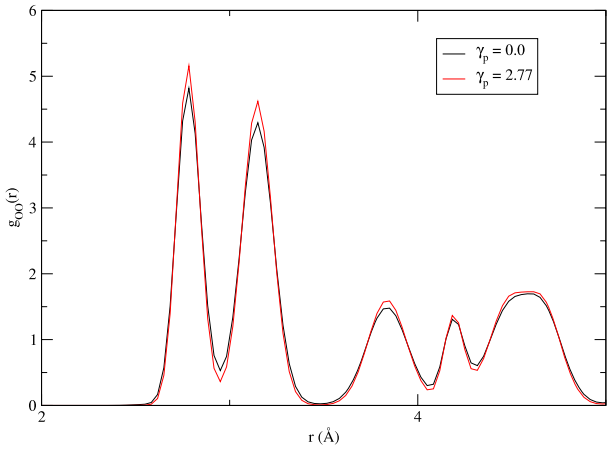

Figure 10. O–O radial distribution function for single-temperature model (black) and two-temperature model with $\gamma_p = 2.77$, averaged across the 20 initial displacement vectors for each value of γ_p.

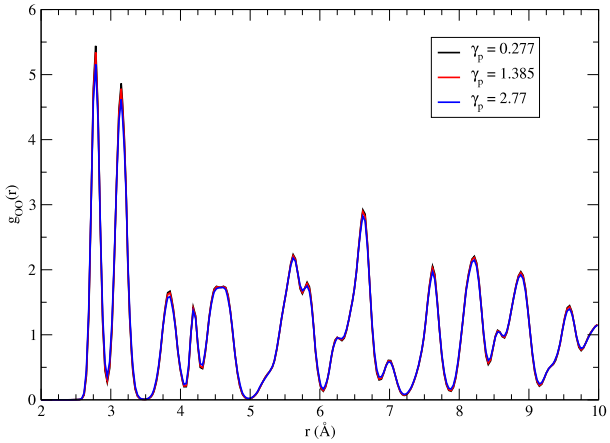

Figure 11. O–O radial distribution function for $\gamma_p = 0.277$, 1.385, and 2.77, averaged across the 20 initial displacement vectors for each value of γ_p.

functions for the displacement of the PKA atom after 10 000 time steps (approximately 16 ps) is shown in figure 9; the mean and standard deviations of the displacement across the 20 vectors considered for each value of γ_p are listed in table 3. It can be clearly seen that the greater the magnitude of the friction coefficient γ_p, the greater the reduction in both the mean displacement and in the standard deviation of the displacements. Moreover, the relative reduction in the standard deviation is larger than the relative reduction in the displacements. This suggests that the path taken by the PKA initially follows the original velocity vector chosen for the PKA, while further away from the formation site of the PKA, displacements are more random in nature.

While the presence of the PKA can induce significant local variations in the structure of the system in the vicinity of the original damage location, the overall impact of the damage cascade caused by the PKA is relatively limited. To observe this, we note the oxygen–oxygen radial distribution function, which is shown for distances of $r < 5$ Å in figure 10 for $\gamma_p = 0$ and 2.77 g mol^{-1} fs^{-1}. Comparing the functions for the two different systems, we note that the locations of the local minima and maxima are essentially unchanged as a function of γ_p. The only difference between the two functions that can be readily observed is that the extrema are 'sharper' for the system with $\gamma_p > 0$, which indicates that the peak heights are higher for the TTM system than for the model without electronic effects. The presence of the electronic subsystem dissipates a portion of the PKA's kinetic energy and reduces the severity of the damage cascade. Comparing these RDFs to the RDF for the system without damage shows the same general behavior for distances $r < 4$ Å, but the two peaks near $r = 4.5$ Å are not observed for the simulations following the damage cascade.

Examining the RDFs for the TTM simulations as a function of γ_p, shown in figure 11, we find that the peak heights actually decrease as a function of γ_p; unlike the high γ_p case shown in figure 10, there is evidence of the two peaks near $r = 4.5$ Å in the RDFs for $\gamma_p = 0.277$ and 1.385 g mol^{-1} fs^{-1}, which suggests that the increase in kinetic energy associated with the higher equilibrium temperatures leads to greater displacements of defect atoms as the friction coefficient increases.

4. Conclusions

We have used a two-temperature model to study cascade damage caused by formation of a PKA atom in the pyrochlore $Gd_2Zr_2O_7$, with particular attention paid to the effect of the electron–ion interaction friction coefficient γ_p on the dynamics and equilibrium properties. Our results show that the ability of the electronic subsystem to act as a heat 'sink' for the PKA has a major impact on the extent and severity of the resulting cascade damage. Some properties, such as PKA displacement distance, show the expected behavior as a function of γ_p. Other properties, such as the final equilibrium temperature or the radial distribution function, show more complicated behaviors with respect to the value of γ_p. This appears to be the result of the greater, but more uniform, heat dissipation caused by the electron–ion interaction, which allows atoms in the two-temperature models to have greater kinetic energies and

vibrational mobility around their equilibrium positions within the crystal lattice.

These results suggest that more accurate determination of the relaxation time of the electron–ion interactions is needed in order to obtain better measurements of the behavior of real materials in a cascade. Further work is also needed to investigate the dependency of the final electronic subsystem temperature on the electronic subsystem mesh refinement. One possible alternative to the use of an electronic mesh may be to consider the electrons contained in each cell as an explicit, time-dependent variable in the simulation. Such an alteration would overcome some of the obstacles associated with the uniform electron density assumed in the current implementation.

An initial extension of this work would be to perform a sensitivity analysis to determine which TTM parameters are responsible for the degree of post-cascade healing seen in the defect analysis. Additionally, quantum calculations are needed to further refine our parameter choices for the electronic specific heat and electron density. Future work should also involve an extension to other waste form materials, particularly in light of recent quantum calculations comparing disordering energies in a range of pyrochlores [8]. Trends in the number of post-cascade defects from MD simulation should make for an interesting comparison with the calculated disordering energies.

Acknowledgments

Sandia National Laboratories is a multiprogram laboratory operated by Sandia Corporation, a Lockheed-Martin Company, for the US Department of Energy under Contract No. DE-AC04-94AL85000.

References

[1] Weber W J, Navrotsky A, Stefanovsky S, Vance E R and Vernaz E 2009 *MRS Bull.* **34** 46
[2] Lumpkin G R 2006 *Elements* **2** 365
[3] Lang M, Lian J, Zhang J, Zhang F, Weber W J, Trautmann C and Ewing R C 2009 *Phys. Rev.* B **79** 224105
[4] Yudinsev S V, Lukinykh A N, Tomilin S V, Lizin A A and Stefanovsky S V 2009 *J. Nucl. Mater.* **385** 200–3
[5] Patel M K, Vijayakumar V, Kailas S, Avasthi D K, Pivin J C and Tyagi A K 2008 *J. Nucl. Mater.* **380** 93–8
[6] Zhang J, Lang M, Lian J, Liu J, Trautmann C, Della-Negra S, Toulemonde M and Ewing R C 2009 *J. Appl. Phys.* **105** 113510
[7] Sickafus K E, Grimes R W, Valdez J A, Cleave A, Tang M, Ishimaru M, Corish S M, Stanek C R and Uberuaga B P 2007 *Nat. Mater.* **6** 217
[8] Jiang C, Stanek C R, Sickafus K E and Uberuaga B P 2009 *Phys. Rev.* B **79** 104203
[9] Rushton M J D, Grimes R W, Stanek C R and Owens S 2004 *J. Mater. Res.* **19** 1603
[10] Moreira P A F P, Devanathan R, Yu J and Weber W J 2009 *Nucl. Instrum. Methods* B **267** 3431
[11] Trachenko K 2004 *J. Phys.: Condens. Matter* **16** R1491
[12] Sickafus K E, Minervini L, Grimes R W, Valdez J A, Ishimaru M, Li F, McClellan K J and Hartmann T 2000 *Science* **289** 748
[13] Cleave A, Grimes R and Sickafus K 2005 *Phil. Mag.* **85** 967–80
[14] Rushton M J D, Stanek C R, Cleave A R, Uberuaga B P, Sickafus K E and Grimes R W 2007 *Nucl. Instrum. Methods* B **255** 151–7
[15] Purton J A and Allan N L 2002 *J. Mater. Chem.* **12** 2923
[16] Chartier A, Meis C, Crocombette J P, Corrales L R and Weber W J 2003 *Phys. Rev.* B **67** 174102
[17] Trachenko K, Dove M T, Artacho E, Todorov I T and Smith W 2006 *Phys. Rev.* B **73** 174207
[18] Caro A and Victoria M 1989 *Phys. Rev.* A **40** 2287
[19] Duffy D M and Rutherford A M 2007 *J. Phys.: Condens. Matter* **19** 016207
[20] Rutherford A M and Duffy D M 2007 *J. Phys.: Condens. Matter* **19** 496201
[21] Duffy D M, Khakshouri S and Rutherford A M 2009 *Nucl. Instrum. Methods* B **267** 3050–4
[22] Phillips C L and Crozier P S 2009 *J. Chem. Phys.* **131** 074701
[23] Ewing R C, Weber W J and Lian J 2004 *J. Appl. Phys.* **95** 5949
[24] Todorov I T, Purton J A, Allan N L and Dove M T 2006 *J. Phys.: Condens. Matter* **18** 2217
[25] Phillips C L, Crozier P S and Magyar R J 2010 *Phys. Rev.* B submitted
[26] Moriga T, Yoshiasa A, Kanamaru F, Koto K, Yoshimura M and Somiya S 1989 *Solid State Ion.* **31** 319
[27] Plimpton S J 1995 *J. Comput. Phys.* **117** 1
[28] Hockney R W and Eastwood J W 1988 *Computer Simulation Using Particles* (Bristol: Adam Hilger–Institute of Physics Publishing)
[29] Plimpton S J, Pollock R and Stevens M J 1997 *Proc. 8th SIAM Conf. on Parallel Processing for Scientific Computing*
[30] Ziegler Z F 2003 The stopping and range of ions in matter (http://www.srim.org)
[31] Zhong Y, Nordlund K, Ghaly M and Averback R S 1998 *Phys. Rev.* B **58** 2361
[32] Rein ten Wolde P, Ruiz-Montero M J and Frenkel D 1996 *J. Chem. Phys.* **104** 9932
[33] Auer S and Frenkel D 2004 *J. Chem. Phys.* **120** 3015